한국해양공학회지 제24권 제1호, pp 1-9, 2010년 2월 (ISSN 1225-0767)

Experimental Study on Nonlinearity Characteristics Near the Free Surface in the Regular Wave Condition

Hae Jin Choi*, Kwang Hyo Jung**, Sungbu Suh**, Hyo Jae Jo*** and Han Suk Choi****

*Hanjin Heavy Industries & Construction Co. Ltd., Busan, Korea
**Department of Naval Architecture and Ocean Engineering, Dong-Eui University, Busan, Korea
***Division of Naval Architecture and Ocean Systems Engineering, Korea Maritime University, Busan, Korea
****Department of Naval Architecture and Ocean Engineering, Pusan National University, Busan, Korea

KEY WORDS: Regular wave, Particle image velocimetry technique, Water velocity, Local acceleration, Convective acceleration, Nonlinearity

ABSTRACT: *A series of experiments employing particle image velocimetry (PIV) technique was conducted to produce benchmark wave kinematics data for regular waves having four different wave slopes in 2-D wave tank. Water velocities and accelerations near the free surface of regular waves were computed from image pair obtained by PIV systems. With the measured wave velocity field, the wave accelerations were computed using a centered finite difference scheme. Both local and convective components of the total accelerations are obtained from experimental data. With increasing the wave slope, the horizontal velocity and the vertical accelerations near the wave crest obtained by PIV technique became larger than theoretical results, which are well-known phenomena of the wave nonlinearity. It is noted that the relative magnitude of convective acceleration to the local acceleration became larger with increasing wave slope.*

1. Introduction

After the middle of the 1990s, oil and gas fields moved into deep water, 900~3000 m. As the search for oil and gas progresses, various concepts should be considered for deep water offshore structures. In calculating dynamics and loads on offshore structures, a precise understanding of ocean wave kinematics is required. Since George Biddell Airy's long and influential article "Tides and Waves", was published in 1845, much research has been done looking for representation of a realistic ocean wave. The understanding of water waves and the associated kinematics has advanced substantially during the last four to five decades. There are a number of experimental observations for regular wave kinematics. In many cases, the agreement between theoretically predicted wave kinematics and experimental observations is reasonably good. To produce a good agreement between theoretical prediction and experimental observation, theoretical equations for periodic waves were developed in the consideration of the effects of viscosity, higher order terms in formulation, and wave-wave interactions. Advanced technologies, such as Laser Doppler Velocimetry (LDV) and Particle Image Velocimetry (PIV), have also improved observations in the laboratory.

There have been many investigations of water wave kinematics. The first realistic description was presented by Stokes (1847). He extended Airy's linear wave theory (1845) to the second order. The second-order Stokes wave theory was then extended to the fifth-order for better accuracy in computing the characteristics of regular waves by De (1955) and Fenton (1985). Chappelear (1961) and Dean (1965) extended this theory to much higher orders with the help of computers. Dean (1970) examined the root-mean-square errors in kinematic and dynamic free surface boundary conditions associated with a number of analytic wave theories and numerical theories and concluded that the calculations of the higher-order Stokes wave theories approach the measured data of wave motion in deep water. A more accurate numerical scheme for computing the characteristics of regular waves including heights ranging up to near breaking was developed by Schwartz (1974) and later extended by Cokelet (1977).

Although the higher order terms for the higher-order Stokes wave equations have been obtained in order to reduce discrepancies between calculated and measured periodic wave kinematics, the predictions of the higher-order Stokes wave theory did not match well with the measurements. The regular wave theories were modified to predict wave kinematics with the following three steps: First, Lo and Dean (1986) modified the linear wave theory by adjusting the depth decaying function $\sinh^{-1}(kd)$ to $\sinh^{-1}(k(d+\eta))$. Second, nonlinear terms are added to wave theories, with viscosity being one. The

Corresponding author Kwang Hyo Jung: Busan Busanjingu Eomkwangro 995, 051-890-2592, khjung@deu.ac.kr

theoretical descriptions noted above have one important point, which is that they all assume wave motion is irrotational, and therefore no vorticity exists throughout the depth of flow fields. However, it is clear from the conduction solution proposed by Longuet-Higgins (1953) that a vorticity profile can exist within the interior of the flow field. There are also a number of experimental observations which appear to support this view. Anastasious et al. (1982) concluded with their observations that the large positive velocities near the surface region were overestimated by the irrotational solution. Swan (1990) considered the effects of a fully diffused vorticity and applied a viscous modification to a third order of wave steepness. He concluded that an irrotational solution overestimates the amplitude of the oscillatory motion in the upper half of the flow field, and underestimates the amplitude in the lower half. However, his viscous modification was only for regular waves of moderate height in water of intermediate depth. Finally, the third step is to impose no mass transfer in the fluid. Gudmestad and Connor (1986) developed the wave theory on the basis of this third step and showed good agreement with experimental results. Sobey (1990) has also reviewed the apparent inconsistency of the regular wave theories to predict the wave kinematics. He referred to Fenton (1985) who pointed out that it was necessary to know the wave speed in order to calculate the wave kinematics.

The objective of this study is to produce the benchmark wave kinematics date set for regular waves having different wave slopes and to provide PIV application model which can obtain the velocity profile and the total acceleration in a fluid region under water waves. The local acceleration can be computed by the time derivative of consecutive velocity profiles, and the convective acceleration can be calculated by the spatial derivative of velocity vectors in the same velocity profile. This study shows that PIV application can be extended to investigate highly nonlinear waves, irregular wave, rouge wave, and so on, which are hard to be computed by theoretical and numerical techniques.

2. Experimental Technique and Conditions

To measure the water particle velocities of regular waves, we conducted a series of experiments using two dimensional wave tank. The wave tank was a 35 m long, 0.91 m wide, and 1.22 m deep glass-walled flume as shown in Fig. 1 and equipped with a permeable wave absorbing 1 : 5.5 sloping beach down-stream. A layer of horsehair was placed on the beach to absorb the wave energy and reduce reflection. Before conducting experiments in this wave tank, we found

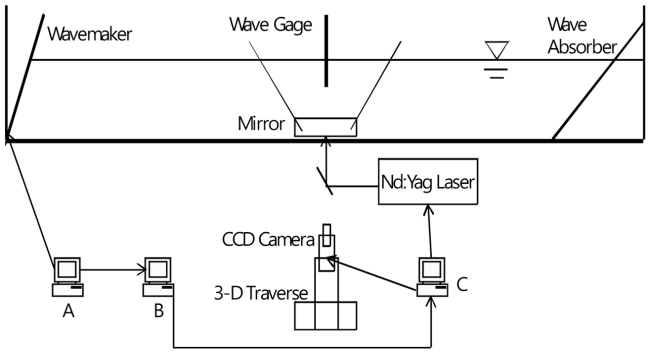

Fig. 1 Schematic sketch of the experimental set-up using the PIV system. Computer A: to control the wavemaker and trigger the PIV system. Computer B: to take data from wave the gages. Computer C: to control the laser and CCD camera

that the reflection coefficient which is the ratio of reflected wave height to incident wave height was 5%. Wave generation was provided by a dry-back, hinged flap wavemaker. The flap is driven by a synchronous servo-motor controlled by a computer and hydrostatically balanced using an automatic near constant force and a pneumatic control system. The double-wired resistant-type wave gages were used to measure the free surface elevation. The signal from the wave gage was converted to voltage and sent to a data acquisition board housed in a computer. The gage was located at the measurement position of velocities to measure the wave elevation. All data from the wave gages was measured at a sampling rate of 100 Hz.

The PIV system was used to map the velocity field in the study. The PIV system used in this study is sketched in Fig. 1. The PIV system and the wavemaker were synchronized by computer A housing a data acquisition board (National Instruments AT-AO-6/10) which generated analog output DC voltage. The timing of laser pulses was controlled by computer B housing the Programmable-Timing-Unit-Board (Fig. 1). The control signals of the PIV system and the wavemaker were synchronized with all the data from the wave gages.

The PIV technique is a non-intrusive, indirect, and whole field method; therefore, no probe was used to disturb the fluid in the experiment. An artificial seeding particle is added for velocity measurement, and thousands of velocity vectors can be obtained simultaneously. A dual-head Spectra-Physics Nd : YAG laser was used as the PIV illumination source in the experiment. The laser contains a crystal harmonic generator to double the 532 nm green light from the original 1064 nm invisible light. The laser has a maximum energy output of 400 mJ/pulse in the 532 nm wavelength, a pulse duration of 10 ns, and a repetition rate of 10 Hz in each head so that 20

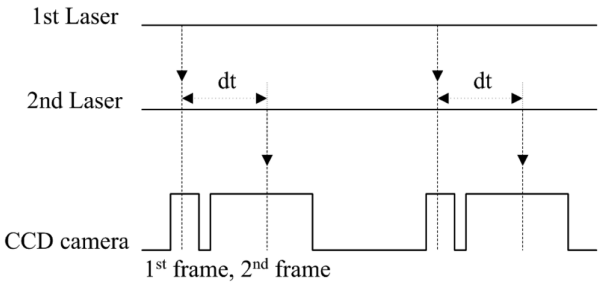

Fig. 2 Double-frame/single-pulsed method

pulses are generated per second. The light sheet optic used a combination of two spherical lenses and one cylindrical lens to generate a thin light sheet (about 1 mm) from the 3 mm diameter laser beam. Vestosint 2157 natural, which is made of polyamide 12, was used as the seeding particle which has a mean diameter of 57 μm and a specific weight of 1.02. The camera used to capture images is a digital CCD (Charge-Coupled Device) camera mounted with a 105 mm f/1.8 micro focal lens set at f/2.8~4.0. It has 1280 × 1024 pixels, a 6.7 μm × 6.7 μm pixel size, 12 bit dynamic range, and 8 Hz framing rate. The PIV images were recorded by the double-frame/single-pulsed method shown in Fig. 2. The main advantage of this technique is to remove the directional ambiguity. The time difference (dt) between the 1st frame and 2nd frame was adjusted to be about 3~5 ms, which was determined by the maximum displacement to be less than a third of the width of the interrogation window size.

The background noise was subtracted before the evaluation of velocity vectors. The complex 2-D fast Fourier transform was calculated from the two small areas (called interrogation windows), and the result was multiplied by its complex conjugate. Then, the inverse FFT was applied to yield the cross correlation function. The use of FFT can simplify and significantly speed up the cross-correlation process of two interrogation windows from a pair of images (Willert and Gharib, 1991). The adaptive multi-pass algorithm was applied to reduce faulty vectors. Firstly, it has calculated a reference velocity vector for each rectangle section which was an initial cell size (four times of an interrogation area). At the next step, this reference velocity vector was used as a cell shift to compute a more accurate vector field. Because this method has shifted an interrogation area to the location where particles moved, the stronger cross-correlation can be taken. Once the velocity vectors have been calculated in the interrogation area (32 × 32 pixels) with a 50% overlap, spurious false vectors were eliminated by the median filter (Westerweel, 1993). The left-over empty spaces were filled-up with interpolated vectors and smoothed by a simple 3 × 3 smoothing filter to reduce noise.

Table 1 The experimental conditions using the PIV system for regular waves

CASE	H (cm)	H_c (cm)	H_t (cm)	T (s)	H/L	ka
Case PR1	4.17	2.05	–2.12	0.90	0.033	0.104
Case PR2	8.13	4.52	–3.61	0.90	0.064	0.202
Case PR3	10.12	5.51	–4.61	0.90	0.080	0.252
Case PR4	12.29	7.27	–5.02	0.90	0.097	0.305

A series of experiments using the PIV system was conducted to measure the particle velocities of regular waves. The set-up is shown schematically in Fig. 1, where x is the horizontal coordinate positive in the direction of wave propagation with $x = 0$ at the wave maker and z is positive upward. The free surface elevations were measured at the location distanced 8 m from wave maker. Four regular wave trains with the same period $T = 0.9$ s were generated with four different wave heights. The velocity fields of regular waves were obtained at 8 m from wavemaker using the PIV system. The water depth in the wave tank was maintained at 90 cm. Table 1 shows the experimental conditions for each regular wave test. Cases PR1, PR2, PR3, and PR4 was tested to understand the nonlinearity of regular wave according to increasing wave height with the same wave period.

3. Experimental Procedure and Data Processing

The generation time of regular waves was varied with the group velocity of the propagating wave based on the design wave period, the water depth, and the distance from the flap wave maker to the target wave gage. To get clean wave signal sets, the overlap of an incident wave and a reflected wave at the target wave gage should be avoided. Using these considerations, regular wave generation time was selected for 50 seconds. Approximately, 55 waves were obtained in the 50 seconds wave generation time. Of the waves, twelve incident waves in steady state were selected to measure the wave particle velocities. The root-mean-square wave heights (H_{rms}) for each case were checked and are shown in Table 2.

$$H_{\mathrm{rms}} = \sqrt{\sum_{i=1}^{N}\left[(H_i - H_{mean})^2/N\right]} \tag{1}$$

Table 2 The RMS wave heights (H_{rms}) of selected experimental regular waves

CASE	Case PR1	Case PR2	Case PR3	Case PR4
cm	0.01	0.02	0.07	0.11
ER_{wave} (%)	0.21	0.23	0.65	0.93

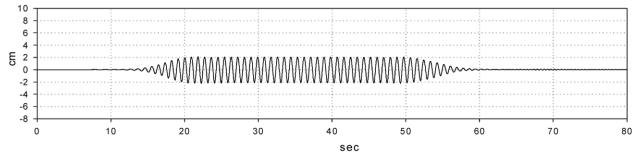

(a) Case PR1

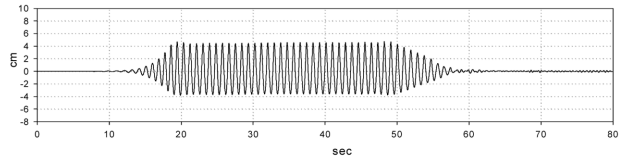

(b) Case PR2

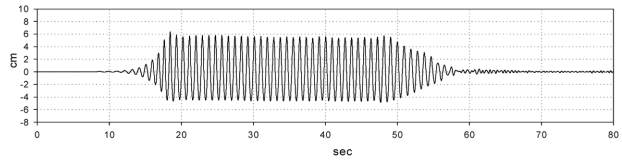

(c) Case PR3

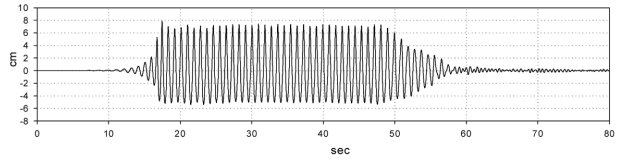

(d) Case PR4

Fig. 3 Time series of regular waves for 4 cases

where H_i represents measured wave height for each wave, Hmean the average wave height of selected regular waves and N the number of selected regular waves.

The error rate of selected regular waves was calculated by the equation (2).

$$ER_{wave}\ (\%) = (H_s/H_{mean}) \times 100 \tag{2}$$

The time series of four regular waves are shown in Fig. 3. The measurements were taken from twelve waves which are reached a steady state and did not include the reflected waves coming back. Using the phase-average method, the mean velocity is obtained. Twelve pairs of images were taken at each phase for twelve different phases for the PIV velocity measurements. The sizes of the fields of view are 127×159 mm^2. The coordinate system is also shown in Fig. 4 with $z = 0$ being the stationary free surface elevation and $x = 0$ the location of wave gage. The 32×32 pixels interrogation windows corresponded to a spatial resolution of 2.07×2.07 mm^2.

The mean velocity is used to analyze regular wave kinematics in this study. The mean velocity was obtained by phase-averaging the measured instantaneous velocities at each phase, i.e.,

$$U_k = \frac{1}{N}\sum_{l=1}^{N} u_k^{(l)} \tag{3}$$

where U_k is the phase-averaged mean velocity, $u_k^{(l)}$ is the k-component velocity obtained from the l^{th} instantaneous velocity measurement, and N the total number of instantaneous velocities at that phase. The RMS horizontal particle velocity was obtained by the equation (4), i.e.

$$U_{rms} = \sqrt{\sum_{i=1}^{N}\left[(U_i - U_k)^2/N\right]} \tag{4}$$

where U_i represents the measured instantaneous water velocity at each interrogation area and N the number of selected regular waves. The RMS values of particle velocities were checked for all cases, and were less than 5% against the phase-averaged mean velocity.

The total acceleration derivative is composed of two terms: the local acceleration which is the change of velocities observed at a point in time and the convective acceleration terms which are the changes of velocities that result due to the motion of the particle. The total acceleration in 2-D is

$$\frac{D\vec{U}}{Dt} = \underbrace{\frac{\partial \vec{U}}{\partial t}}_{Local\ acceleration} + \underbrace{\vec{U} \bullet \nabla \vec{U}}_{\substack{Convective \\ acceleration}} \tag{5}$$

The local acceleration fields were computed by applying a centered finite difference scheme to measured velocity fields. Each regular wave of the PIV measurements consists of twelve phases or twelve field views per wave length. Since the wave period was 0.9 s, the time interval between each PIV phase was 0.075 s. The local acceleration near the wave crest could not be obtained because of no velocity data near the free surface corresponding to the previous and next phases. This missing local acceleration can be reduced with smaller time steps between phases. The convective acceleration fields were computed by applying a centered finite difference scheme with 6 mm grid spacing.

4. Experimental Results

A series of experiments were conducted to obtain the particle velocity fields using the PIV system for four different wave slope regular waves. Since one wavelength regular wave consists of twelve velocity fields, i.e. the twelve phases per wave length, the vertical and horizontal components of particle velocity under the wave crest, the wave trough, the zero-up crossing point and the zero-down crossing point for regular waves were able to obtained. The wave crest and trough are defined as the highest elevation point and the lowest elevation point of the wave, respectively. If the wave elevation goes down according to the direction of progressive wave propagation and passes the still water level, the point

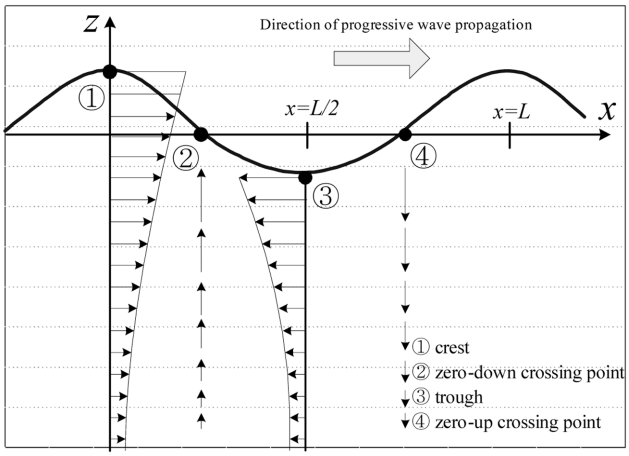

Fig. 4 Definition sketch for the crest, trough, zero-up and down crossing point of water wave and distribution of water particle velocities in progressive waves

of wave elevation can be called the zero-down crossing point. The zero-up crossing point of a wave is the opposite, i.e. the wave elevation goes up. The definitions of wave crest, wave trough and wave zero crossing points are shown in Fig. 4. Measured velocities are presented in normalized value; i.e., the measured vertical position Z is normalized by water depth (d) and the horizontal velocity (u or V_x) and the vertical velocity (w or V_z) are normalized by wave phase velocity (v_p).

Horizontal velocities of Case PR1 ($ka = 0.104$) according to the vertical measuring positions under the wave crest and trough are shown in Fig. 5(a) and (b), respectively. The measured data are presented with the results from the linear theory and the third-order Stokes theory. In general, both analytical results matched very well with experimental data. It is also seen in Fig. 5(a) that the linear theory and the third-order Stokes wave theory are almost identical due to the small amplitude of Case PR1. Compared with Fig. 5(a) and (b), the measured velocities under the trough are, approximately, 4% larger than those of the third-order Stokes wave theory, but measured velocities under the crest are agreed well with theory results.

Figs. 5(c) and (d) present the horizontal velocities under the wave crest and trough for Case PR2 ($ka = 0.202$), respectively. Compared to Case PR1, the experimental results of Case PR2 agree excellently with analytical solutions although they have twice the wave slope. Both analytical solutions are equal to each other with 1.0% difference at the wave crest as shown in Fig. 5(a). It is more noticeable compared to Case PR1 that the values of Case PR2 measured data under the trough is slightly larger, i.e. 5.0%, than those of the 3rd-order Stokes wave theory and those of measured velocity under the crest at the corresponding measured vertical positions as shown in Fig. 5(d).

Figs. 5(e) and (f) show the horizontal velocities under the wave crest and trough for Case PR3 ($ka = 0.252$), respectively. The experimental results of Case PR3 are in good agreement with analytical solutions, although there is a 2.5 times larger wave slope than that of Case PR1. Compared with Case PR1 and Case PR2, however, analytical solutions from both of the linear extrapolation and the third-order Stokes wave theory are very similar with 2.0% difference at the wave crest as shown in Fig. 5(e). It can be seen by comparing with Case PR1, Case PR2 and Case PR3 the values of Case PR3 measured data under the trough is 9.6% larger than those from the third-order Stokes wave theory and those of measured velocity under the crest at the corresponding measured vertical positions as shown in Fig. 5(f).

The horizontal velocities of Case PR4 ($ka = 0.305$) under the wave crest and trough are presented in Fig. 5(g) and (h), respectively. The measured data of Case PR4 agree well with both the solutions of linear theory and the third-order Stokes wave theory below the mean sea level. The measurements above the mean sea level are larger than those of linear wave theory and the third-order Stokes wave theory as shown in Fig. 5(g). The wave slope of Case PR4 is 3.7 times larger than that of Case PR1. It is seen in Fig 5(g) that the solutions above the free surface of the third-order Stokes wave theory are maximum 3.8% larger than those of linear theory. Note that the horizontal velocity of Case PR4 is larger than that of the 3rd order Stokes wave theory. The trough horizontal velocities for Case PR4 are presented in four vertical measuring positions under the wave trough due to the limitation of field of view (FOV) size. Compared with Fig. 5(g) and (h), the magnitudes of measured data below the trough are very similar to those of measured velocity below the crest at the corresponding vertical measuring positions, unlike Case PR1, Case PR2 and Case PR3. Fig. 6 presents the vertical velocities under the wave zero-up and down crossing point for Case PR1, Case PR2, Case PR3, and Case PR4, respectively, with the good agreement between PIV measurements and the results of the third-order Stokes wave theory.

The local acceleration fields were computed based on PIV measurements of the fluid velocities under the regular wave crest. The numerical scheme used for computation was a centered finite difference method with 0.075 s. The measured local accelerations are presented with normalized by the gravity acceleration. Fig. 7 shows the vertical local accelerations under the wave crest for four regular waves.

The experimental results of Case PR1 and Case PR2 show strong agreement with the analytical solutions as shown in

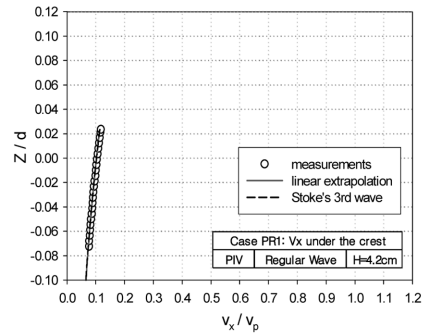

(a) Case PR1(under wave crest)

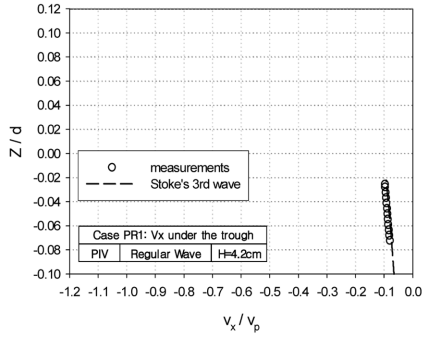

(b) Case PR1(under wave trough)

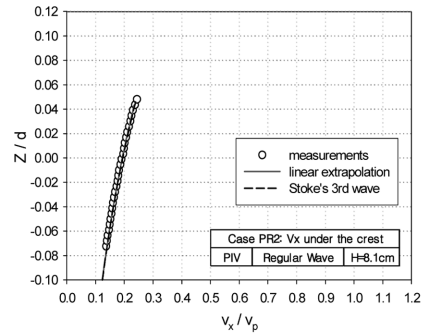

(c) Case PR2(under wave crest)

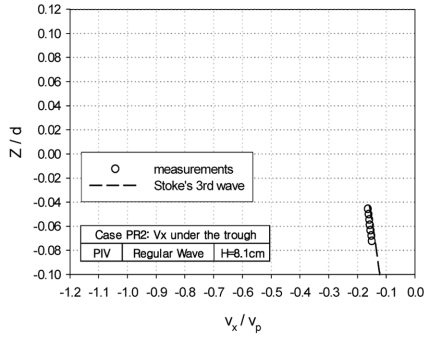

(d) Case PR2(under wave trough)

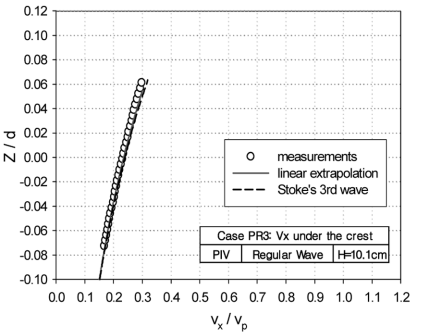

(e) Case PR3(under wave crest)

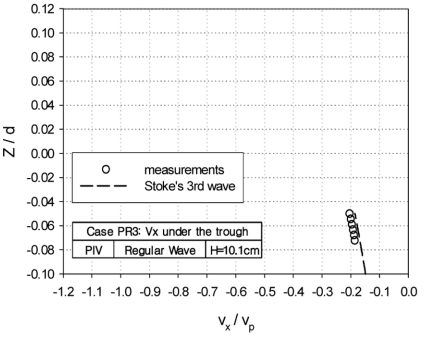

(f) Case PR3(under wave trough)

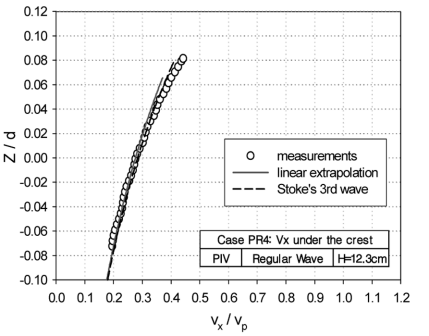

(g) Case PR4(under wave crest)

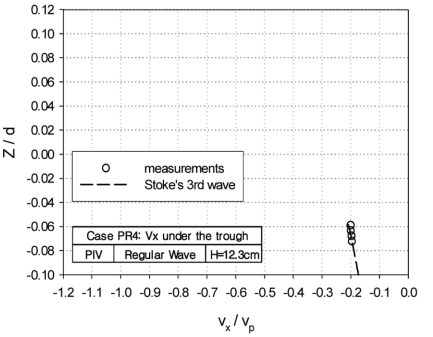

(h) Case PR4(under wave trough)

Fig. 5 Comparison with horizontal velocities for 4 cases

Fig. 7(a) and Fig. 7(b), respectively. However, analytical solutions from both the linear extrapolation and the third-order Stokes wave theory predict the vertical local accelerations for Case PR3 are larger than the computed values based on PIV measurement as shown in Fig. 7(c). In Fig. 7(d), the vertical local accelerations computed based on PIV measurement

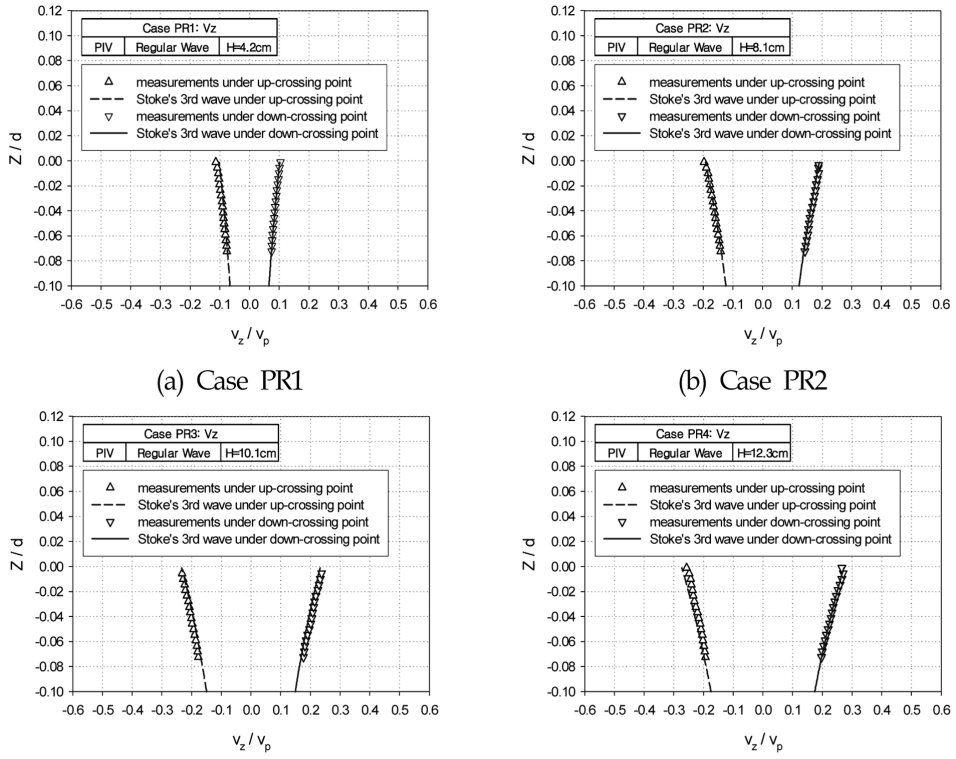

(a) Case PR1 (b) Case PR2

(c) Case PR3 (d) Case PR4

Fig. 6 Comparison with vertical velocities under wave zero-up and zero-down crossing point for 4 cases

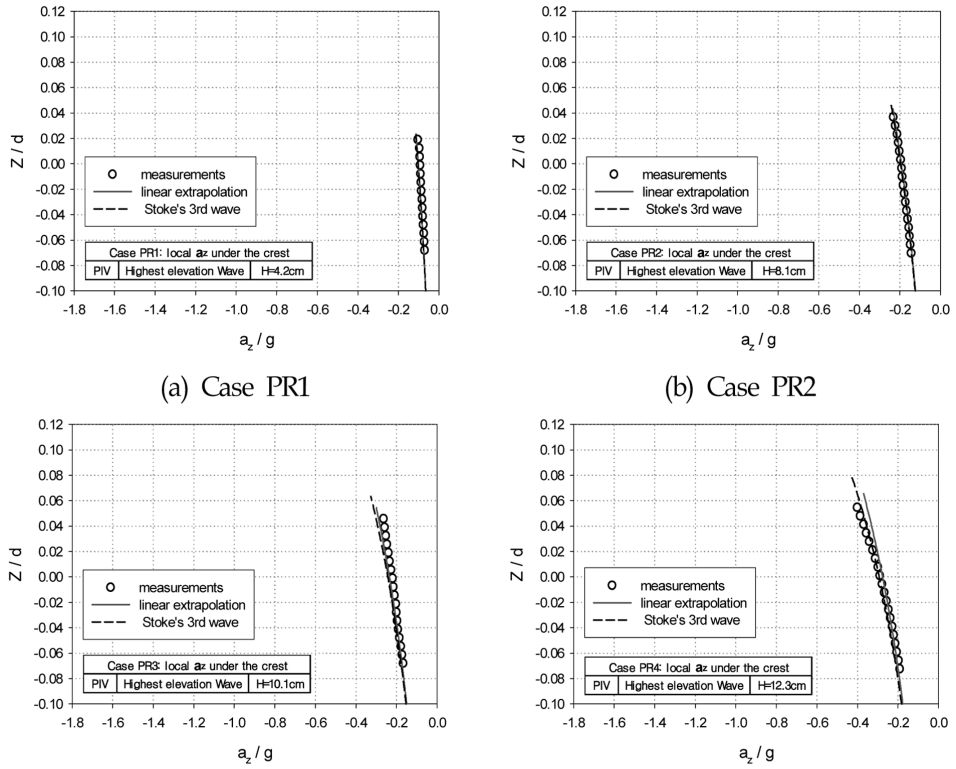

(a) Case PR1 (b) Case PR2

(c) Case PR3 (d) Case PR4

Fig. 7 Comparison of vertical local accelerations under the wave crest

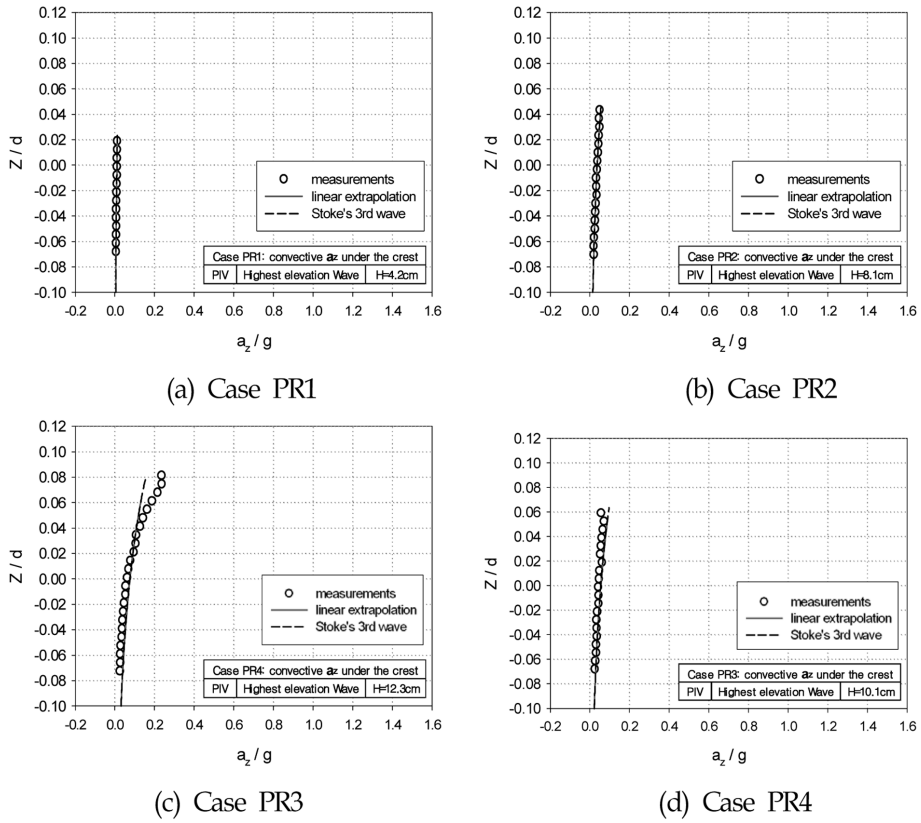

(a) Case PR1 (b) Case PR2

(c) Case PR3 (d) Case PR4

Fig. 8 Comparison of vertical convective accelerations under the wave crest

above the free surface level for under the wave crest of Case PR4 are larger than those of both linear extrapolation and the third-order Stokes wave theory. Jensen et al. (2001) measured the velocities and accelerations in the periodic wave with the wave slope of $ka = 0.16$. They had the relative standard deviation of 0.6% for the velocity measurements and 2% for the acceleration measurements with a time step 0.06 s. The RMS velocity was observed as less 1.2% in Case PR3 ($ka = 0.252$). The better accuracy in velocity and acceleration could be required less interrogation area and less time step between consecutive velocities.

The convective acceleration was computed based on the PIV measurements of the particle velocities under the regular wave crest using a centered finite difference method with 6 mm spatial resolution. Fig. 8 presents the vertical convective accelerations under the wave crest for four regular waves. The experimental results of Case PR1, Case PR2, and Case PR3 agree well with the solutions of the linear extrapolation and the third-order Stokes wave theory as shown in Fig. 8(a) and Fig. 8(b), respectively. It is noted in Fig. 8(d), Case PR4, which the vertical convective acceleration computed from measured velocities, was suddenly increased near the wave crest and larger than that of the linear extrapolation and the third-order Stokes wave theory. It is possible to be the effects of the wave nonlinearity are more significant as the wave steepness increases.

5. Concluding Remarks

Regular wave kinematics, including water elevation, velocity, local acceleration, and convective acceleration were investigated experimentally employing the particle image velocimetry (PIV) technique. The regular waves of four different wave slopes were generated in the 2-D wave tank. The velocities under the wave crest, wave trough, and wave zero crossing points were measured using the PIV system and compared with solutions of the third-order Stokes wave theory and extrapolation based on the Airy wave theory. The local accelerations and convective accelerations of regular waves were computed from PIV measurements with the centered finite difference scheme.

With increasing the wave slope, the horizontal velocity and the vertical accelerations near the wave crest obtained by PIV technique became larger than theoretical results, which are well-known phenomena of the wave nonlinearity. It is noted that the relative magnitude of convective acceleration to the

local acceleration became larger with increasing wave slope. It expects that the behavior of convective acceleration term for steeper waves and extreme waves is investigated to understand the highly nonlinear wave and estimate the wave loading on ocean structures under the severe sea condition with better accuracy.

Acknowledgement

This paper was supported by Dong-Eui University Research Grant in 2008 (2008AA196).

References

Airy, G.B. (1845). "Tides and Waves", Encyclopedia Metropolitana, London, 5, pp 241-396.

Anastasious, K., Tickel, R.G. and Chaplin, J.R. (1982). "Measurements of Particle Velocities in Laboratory-scale Random Waves", Coastal Engineering, Vol 6, pp 233-254.

Chapplear, J.E. (1961). "Direct Numerical Calculation of Nonlinear Ocean Waves", Journal of Geophysical Research, Vol 66, No 2, pp 501-508.

Cokelet, E.D. (1977). "Steep Gravity Waves in Water of Arbitrary Uniform Depth", Philosophical Transactions of the Royal Society of London Series A Mathematical Physical and Engineering Sciences, Vol 286, No 1335, pp 183-230.

De, S.C. (1955). "Contributions to the Theory of Stokes Waves", Proceedings of Cambridge Philosophical Society, Vol 51, pp 713-736.

Dean, R.G. (1965). "Stream Function Representation of Nonlinear Ocean Waves", Journal of Geophysical Research, Vol 70, No 18, pp 4561-4572.

Dean, R.G. (1970). "Relative Validities of Water Wave Theories", Journal of Waterways Harbors and Coastal Engineering Division, ASCE, Vol 96, No 1, pp 105-119.

Fenton, J.D. (1985). "A Fifth-order Stokes Theory for Steady Waves", Journal of Waterway, Port, Coastal, and Ocean Engineering, ASCE, Vol 111, No 2, pp 216-234.

Gudmestad, O.T. and Connor, J.J. (1986). "Engineering Approximations to Nonlinear Deepwater Waves", Applied Ocean Research, Vol 8, No 2, pp 76-88.

Jensen, A., Sveen, J.K., Grue, J., Richon, J.-B. and Gray, C. (2001). "Accelerations in Water Waves by Extended Particle Imagine Velocimetry", Experiments in Fluids, Vol 30, No 5, pp 500-510.

Lo, J.M. and Dean, R.G. (1986). "Evaluation of a Modified Stretched Linear Wave Theory", Proceedings of the 20th Coastal Engineering Conference, pp 522-525.

Longuet-Higgins, M.S. (1953). "Mass Transport in Water Waves", Journal of Philosophical Transactions of the Royal Society of London Series A-Mathematical Physical and Engineering Sciences, Vol 245, No 903, pp 535-581.

Schwartz, L.W. (1974). "Computer Extension and Analytic Continuation of Stokes' Expansion for Gravity Waves", Journal of Fluid Mechanics, Vol 62, pp 553-578.

Sobey, R.J. (1990). Wave Theory Predictions of Crest Kinematics, In: Tørum, A. and Gudmestad, O.T. (Eds.) Water Wave Kinematics, NATO ASI Series, Kluwer, Dordrecht, The Netherlands, pp 215-231.

Stokes, G.G. (1847). "On the Theory of Oscillatory Waves", Trans. Cambridge Philosophical Society, Vol 8, pp 441-455.

Swan, C. (1990). A Viscous Modification to the Oscillatory Motion Beneath a Series of Progressive Gravity Waves, In: Tørum, A. and Gudmestad, O.T. (Eds.) Water Wave Kinematics, NATO ASI Series, Kluwer, Dordrecht, The Netherlands, pp 313-329.

Westerweel, J. (1993). Digital particle image velocimetry–Theory and application, Ph.D Dissertation, Delft University, The Netherlands.

Willert, C.E. and Gharib, M. (1991). "Digital Particle Image Velocimetry", Experiments in Fluids, Vol 10, No 4, pp 181-193.

2009년 1월 29일 원고 접수
2010년 2월 18일 심사 완료
2010년 2월 18일 게재 확정